Steel and Composite Structures, *Vol. 16, No. 3 (2014) 305-323*
DOI: http://dx.doi.org/10.12989/scs.2014.16.3.305

Simulations of PEC columns with equivalent steel section under gravity loading

Mahbuba Begum * and Debaroti Ghosh

Department of Civil Engineering, Bangladesh University of Engineering and Technology (BUET), Dhaka, Bangladesh

(*Received September 21, 2012, Revised August 29, 2013, Accepted October 30, 2013*)

Abstract. This paper presents numerical simulations of partially encased composite columns (PEC) with equivalent steel sections. The composite section of PEC column consists of thin walled welded H- shaped steel section with transverse links provided at regular intervals between the flanges. Concrete is poured in the space between the flanges and the web plate. Most of the structural analysis and design software do not handle such composite members due to highly nonlinear material behavior of concrete as well as due to the complex interfacial behaviour of steel and concrete. In this paper an attempt has been made to replace the steel concrete composite section by an equivalent steel section which can be easily incorporated in the design and analysis software. The methodology used for the formulation of the equivalent steel section is described briefly in the paper. Finite element analysis is conducted using the equivalent steel section of partially encased composite columns tested under concentric gravity loading. The reference test columns are obtained from the literature, encompassing a variety of geometric and material properties. The finite element simulations of the composite columns with equivalent steel sections are found to predict the experimental behaviour of partially encased composite columns with very good accuracy.

Keywords: composite; columns; equivalent; steel; partially; encased; finite; element

1. Introduction

The effective use of a combination of steel with materials such as concrete can substantially improve the behaviour and cost efficiency of columns used in the construction of mid-rise and high-rise buildings, as compared to using steel-only columns. A partially encased composite (PEC) section refers to a welded H–shaped steel section with concrete infill between the flanges. In Europe, in the early 1980s, PEC columns and beams were introduced using standard-sized rolled steel sections. In 1996, the Canam Group in North America proposed a PEC column section constructed from a thin–walled built–up steel shape with transverse links provided at regular intervals to restrain local buckling as shown in Fig. 1. Using a built–up steel section instead of a standard shape provides the designer with more flexibility when sizing the column cross-section. Moreover, thin steel plates were intentionally specified to obtain a more cost effective column by increasing the contribution of concrete in the load carrying capacity of the column. These factors

*Corresponding author, Ph.D., E-mail: mahbuba@ce.buet.ac.bd

http://www.techno-press.org/?journal=scs&subpage=8 ISSN: 1229-9367 (Print), 1598-6233 (Online)

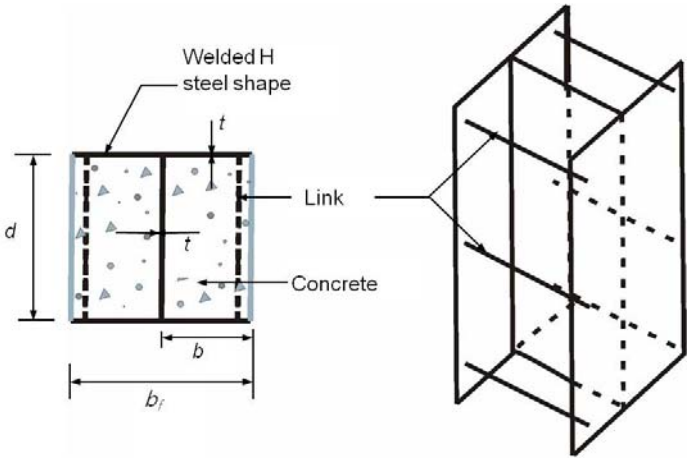

Fig. 1 Partially encased composite column with thin-walled built-up steel section, (a) column cross-section and (b) 3d view of the steel configuration

have made PEC columns constructed with built-up shapes more attractive than those constructed with standard sections.

Extensive experimental research has been performed in Ecole Polytechnique de Montréal (Tremblay *et al*. 1998, Chicoine *et al*. 2000, 2003 and Bouchereau and Toupin 2003) on small- and large-scale PEC column specimens under concentric and eccentric loading conditions. The results of these experimental investigations on PEC columns indicated that the behaviour of this composite column is significantly affected by the local instability of the thin steel flanges. The failure of the composite columns occurred by a combination of local buckling of the steel flanges between the transverse links, yielding of the steel and crushing of the concrete. Usually local buckling occurred at or near the peak load, depending on the slenderness of the flange plates and the link spacing. The influences of high performance materials on the behaviour of these columns have also been investigated experimentally by Prickett and Driver (2006) at the University of Alberta. The failure of the specimens with high strength concrete was found to be less ductile, although addition of steel fibers helped increase the ductility of the failure. However, decreasing the link spacing increased the ductility of the failure. The degree of confinement of concrete in the steel section was found to be low and did not affect the axial load capacity of the columns, as reported by Prickett and Driver (2006). Chen *et al*. (2010) carried out tests and numerical simulations on thin walled PEC columns subjected to axial and cyclic horizontal loads. Their study reveals that though local buckling of thin plate of H steel is a crucial factor, when the compressive axial load does not surpass the encased steel capacity, the PEC column could behave quite well under cyclic horizontal loads. The efficiency of this new composite column as a part of steel plate shear wall has been explored by Deng *et al*. (2008) and Dastfan (2011) through extensive large scale experimental investigations.

Numerical simulations on partially encased composite columns have been performed by Maranda (1998), Chicoine *et al*. (2002) and Begum *et al*. (2007). Maranda (1998), simulated the series of tests on PEC stub columns performed by Tremblay *et al*. (1998) using the computer

program MEF. Only a quarter cross–section was modelled using shell elements for the steel plate, solid elements for the concrete and beam elements for the transverse links. Good agreement was observed between the numerical and the experimental results. However, the model developed by Maranda (1998) was not capable of predicting the post-peak responses of the test specimens. Chicoine *et al*. (2002) performed a finite element analysis using ABAQUS/Standard (HKS 2003) to reproduce numerically the behaviour of the composite column under axial compression only. Similar to the numerical study performed by Maranda (1998), Chicoine *et al*. (2002) also modelled a quarter of the column cross–section with a length of one link spacing. The finite element model was developed using shell elements for the steel section, brick elements for concrete and beam elements for the transverse links. Two node spring elements were used to represent the interaction between steel and concrete at their common interface. The finite element model developed by Chicoine *et al*. (2002) provided a very good representation of the capacity and load versus displacement response of short PEC test specimens (Tremblay *et al*. 1998 and Chicoine *et al*. 2000) up to the ultimate load. The post-peak response of the columns was obtained only over a short deformation range due to convergence problems experienced by the numerical model. This can be attributed to the inadequacy of the implicit solution method for representing the highly nonlinear post-peak behaviour. The researchers identified significant challenges in simulating the local instability of the thin flanges and the triaxial behaviour of the partially confined concrete in the column. Begum *et al*. (2007) were able to overcome these challenges in the finite element model through the implementation of a dynamic explicit formulation along with a damage plasticity model for concrete and a contact pair algorithm at the steel-concrete interface. A complete finite element model including the full cross-section and entire length of the column was developed using the explicit module of ABAQUS finite element code. The model is applicable for concentric as well as eccentric loads. The steel plates were modelled using four node shell elements. Eight-node brick elements were used for concrete and beam elements for transverse links. The developed model was applied successfully to reproduce the behaviour of 34 PEC columns from five experimental programs. The model was able to trace a stable and complete load-strain history accurately for PEC columns with small and large cross-sections, constructed with normal strength, high strength and steel fibre reinforced high strength concrete, and tested under concentric and eccentric loads. The model reliably reproduced the peak load, axial deformation at the peak load, the post-peak behaviour and the failure mode observed in the tests. The interaction between the steel and concrete and their separation at the common interface because of the local instability of the flange was successfully represented in the finite element analyses. However, despite of the accuracy, the composite finite element model developed by Begum *et al*. (2007) is very sophisticated due to the presence of two dissimilar materials. Moreover, the modeling of the interfacial behaviour between steel and concrete requires extensive calculations as well as skilled and experienced users. Due to, these complexities most of the structural analysis and design software do not handle such composite members. In this paper an attempt has been made to simulate the behaviour of this steel concrete composite section using an equivalent steel section which can easily be incorporated in the design and analysis software.

2. Objectives and scope

The primary objective of this study is to formulate an equivalent steel section for thin-walled PEC columns which can accurately simulate the behaviour of the actual composite section. The

equivalent steel section of PEC column is to be formulated using the methodology proposed by Marinopoulou *et al*. (2007) with some modifications. The method developed by Marinopoulou *et al*. (2007) was mainly for partially encased composite sections with fabricated shapes, typically used in Europe. The method is to be modified to incorporate the local instability of the thin flanges in PEC columns. This study also aims to conduct a finite element analysis using the fictitious section of PEC columns to assess the accuracy and reliability of the proposed steel section. PEC test columns from the published literature with a wide variety of geometric and material properties are selected for the finite element analysis.

3. Methodology for formulating the equivalent steel section

The formulation of equivalent cross-section of double-symmetrical partially encased composite steel-concrete column is based on three equivalence criteria: compression resistance and bending stiffness about the two principal axes. The fictitious steel cross-section, as shown in Fig. 2, consists of the actual steel cross-section and two additional pairs of plates, one perpendicular to the web at mid-height and one perpendicular to the flanges at mid-width. Plate dimensions are chosen to match the compression resistance and principal bending stiffness of the composite section. Furthermore, the fictitious steel section is constrained to contain the entire actual steel section.

3.1 Equivalence in compression resistance

The compression resistance of a composite steel-concrete cross section comprises of the plastic resistance of the steel cross-section, steel links and the concrete. The total area of the fictitious cross-section represents the area of the initial steel cross-section and the additional plates.

$$P_{actual} = A_{se} f_s + A_c f_c \tag{1a}$$

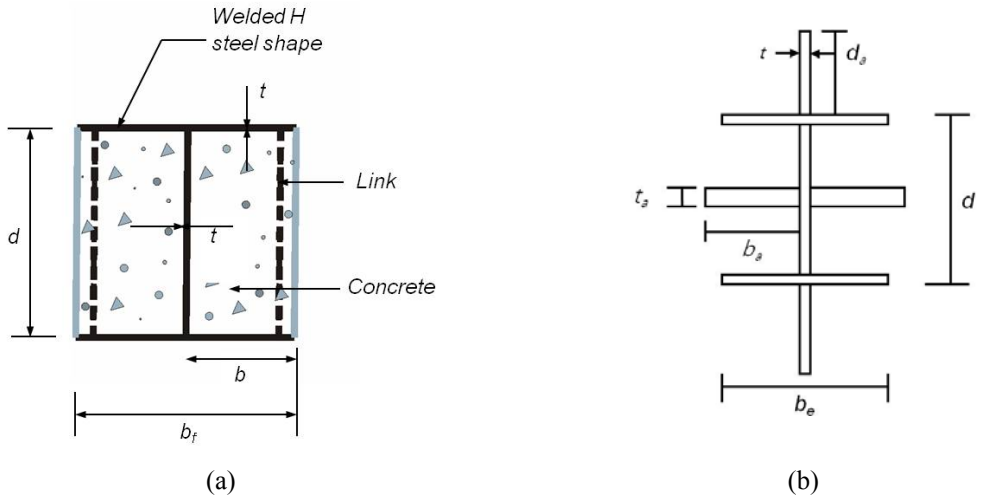

(a) (b)

Fig. 2 Equivalent steel section for PEC column, (a) actual cross-section, (b) equivalent steel section

$$P_{fictit} = \left(A_{se} + A_a\right) f_s \tag{1b}$$

Here, A_{se} = effective area of the steel shape including the I section and the links
A_a = total steel area of the additional steel plates in fictitious section
f_s = design stress of steel
f_c = design stress of concrete

The effective area of a non-compact steel section can be defined as

$$A_{se} = \left(d - 2t + 2b_e\right) t \tag{2}$$

Here, d = overall depth of the cross section
t = thickness of the steel plates
b_e = total effective width of the flange = $b_f / (1+\lambda_p^{2n})^{1/n} \leq b_f$

where

$$\lambda_p = \frac{b}{t}\sqrt{\frac{12\left(1-\nu_s^2\right)F_y}{\pi^2 E_s k}}$$

$$k = \frac{0.9}{(s/b_f)^2} + 0.2(s/b_f)^2 + .75 \quad \left(.5 \leq s/b_f \leq 1\right)$$

Here, s = transverse link spacing
b_f = full width of a flange plate
λ_p = slenderness parameter
E_s = elastic modulus of steel
ν_s = poisson's ratio of steel
n = 1.5 as proposed by Chicoine *et al*. (2002)

Considering the condition of equivalence in compression resistance and the relations in Eqs. (1a)-(1b), it is obtained

$$A_a = A_c \frac{f_c}{f_s} = A_c m_{cd} \tag{3}$$

Here, m_{cd} = design stress ratio for concrete-to-steel

The total area of the composite cross-section comprises the equivalent steel cross section A_{se} and concrete section A_c.

$$b_f d = A_{se} + A_c \tag{4}$$

Dividing Eq. (2) by $b_f d$ and introducing the non dimensional parameters ρ'_{se} and a positive constant q_x^2

$$\frac{A_a}{b_f d} = m_{cd}\rho'_{se} = q_x^2 \tag{5}$$

The total cross-sectional area of the four additional plates in the fictitious section as shown in Fig. 2 is

$$A_a = 2b_a \times t_a + 2d_a \times t \tag{6}$$

which after normalization by $b_f d$ and introduction of normalized plate dimensions β, η, χ and γ becomes

$$\frac{A_a}{b_f d} = (2\beta)\eta + (2\chi)\gamma \tag{7}$$

where, $\beta = b_a / b_f$; $\eta = t_a / d$; $\chi = d_a / d$ *and* $\gamma = t / b_f$.

Since Eqs. (5) and (7) are identical in left hand sides, the outcome is

$$q_x^2 = (2\beta)\eta + (2\chi)\gamma \tag{8}$$

Here the unknowns are β, η and χ on the left side and the combined geometric and material parameters of the actual cross-section enter through the constants γ and q_x^2.

3.2 Equivalence in stiffness about the major axis

The flexural stiffness about the major axis y-y of the actual composite steel-concrete cross-section and its fictitious purely steel counterpart are given by

$$(EI)_{y,actual} = E_{se} I_{se,y} + E_{ce} I_{c,y} \tag{9a}$$

$$(EI)_{y,fictit} = E_{se} I_{se,y} + E_{se} I_{a,y} \tag{9b}$$

Here, E_{se} and E_{ce} are the effective elastic modulous of steel and concrete respectively. $I_{se,y}$, $I_{c,y}$ and $I_{a,y}$ are the moment of inertia about minor axis for actual steel section, concrete and additional steel plates respectively. To enforce the condition of equivalence in major-axis stiffness, solving for $I_{a,y}$ and introducing the concrete-to-steel ratio of elasticity moduli

$$I_{a,y} = \left(\frac{E_{ce}}{E_{se}} \right) \times I_{c,y} = m_e I_{c,y} \tag{10}$$

In reference to Fig. 2(a)

$$\frac{b_f d}{12} \equiv I_{se,y} + I_{c,y}$$

and $I_{se,y} \equiv A_{se} r_{se,y}^2$

Therefore, Eq. (10) may be written as

$$I_{a,y} = m_e \left(\frac{b_f d^3}{12} - A_{se}\, r_{se,y}^2 \right) \tag{11}$$

After normalization of Eq. (11) by dividing it with $b_f d^3 / 12$ and using q_y^2 as a positive constant to sum up the effects of the geometry and material properties of the actual cross section, the final equation is

$$\left(\frac{12 I_a}{b_f d^3} \right) = m_e (1 - 3\rho_{se} \times \lambda_{se,y}^2) = q_y^2 \tag{12}$$

Here, $\lambda_{sa,y} = 2(r_{ay} / d)$ and $\rho_{se} = A_{se} / b_f d$

The additional major-axis flexural stiffness of the fictitious cross-section as a function of the dimensions of the additional plates is given by

$$I_a = \left(2\frac{b_a t_a^3}{12}\right) + \left(\frac{t}{12}\right) \times \{(2d_a + d)^3 - d^3\}$$

This, after normalization with $(b_f d^3 / 12)$ and introduction of the non-dimensional geometric properties β, η, χ, and γ, yields

$$\left(\frac{12 I_{a,y}}{b_f d^3}\right) = (2\beta)\eta^3 + \gamma\{(2\chi + 1)^3 - 1\} \tag{13}$$

Since Eqs. (12) and (13) have identical left-hand sides

$$(2\beta)\eta^3 + \gamma\{(2\chi + 1)^3 - 1\} = q_y^2 \tag{14}$$

Here the unknowns are β, χ on the left side and the combined geometric and material attributes of the actual cross-section enter through the constants γ and q_y^2.

3.3 Equivalence in stiffness about minor axis

The treatment of major axis stiffness equivalence presented in the previous subsection is repeated here in shorthand for the minor-axis case. First, minor-axis counterpart of Eq. (11)

$$I_{a,z} = m_e\left(\frac{b_f d^3}{12} - I_{se,z}\right) = m_e\left(\frac{b_f d^3}{12} - A_{se}\, r_{se,z}^2\right) \tag{15}$$

After normalization of Eq. (15) by dividing it with $b_f d^3 / 12$ and using q_z^2 as a positive constant the obtained equation is

$$\left(\frac{12 I_{a,z}}{b_f d^3}\right) = m_e\left(1 - 3\rho_{se} \times \lambda_{se,z}^2\right) = q_z^2 \tag{16}$$

Here, $I_{se,z} = 2r_{az} / d$ and $\rho_{se} = A_{se} / b_f d$

Similarly for the additional elements of the fictitious steel cross-section, one obtains the counterpart of Eq. (13)

$$\left(\frac{12 I_{a,z}}{b_f d^3}\right) = \left\{\{(2\beta + \gamma)^3 - \gamma^3\}\eta + (2\chi)\gamma^3\right\} \tag{17}$$

Since Eqs. (16) and (17) have identical left-hand sides, the outcome is

$$\left\{\{(2\beta + \gamma)^3 - \gamma^3\}\eta + (2\chi)\gamma^3\right\} = q_z^2 \tag{18}$$

Here the unknowns are β, χ on the left side and the combined geometric and material attributes of the actual cross-section enter through the constants γ and q_z^2.

In order to transform the actual section in to fictitious section, three non-linear equation Eq. (8), Eqs. (14) and (18) were developed. Three non-dimensional parameters, q_x^2, q_y^2 and q_z^2 describe the additional compression resistance, major-axis stiffness, and minor-axis stiffness, respectively, due to concrete and links. These equations must be solved for the three non-dimensional unknowns β, χ and η to determine the dimensions of the additional steel plate's b_a, t_a, and d_a in the fictitious cross-section.

4. Reference test columns

A total of 15 short PEC columns constructed with normal and high strength concrete tested under concentric gravity loads are selected for finite element analysis with equivalent steel section. The lists of these specimens, along with their geometric properties, are given in Table 1. Fig. 3 shows the cross-sections and steel side elevations of a typical test column. Specimens C-1 to C-7 were tested during the initial phase of the research program by Tremblay *et al*. (1998) to study the behaviour of these columns under concentric gravity loading. Specimen C-1 is not included in the numerical analysis because it is a prototype column having different characteristics. In this specimen, stiff bent bars were used as transverse links instead of straight bars that are usually used in Canam-type PEC columns. Specimens C-2 to C-7, which were modelled numerically, had square cross-sections of 300 mm × 300 mm and 450 mm × 450 mm, and a length equal to 5*d*,

Table 1 Geometric properties of reference test specimens

Reference	Spec. design.	Plate size $b_f \times d \times t$ (mm)	Length L (mm)	Plate slenderness ratio b/t	Link		
					Spacing		Diameter Φ (mm)
					S (mm)	Ratio of d	
Tremblay *et al*. (1998)	C-2	450 × 450 × 9.70	2250	23	225	0.5d	12.7
	C-3	450 × 450 × 9.70	2250	23	337.5	0.75d	12.7
	C-4	450 × 450 × 9.70	2250	23	450	1.0d	12.7
	C-5	450 × 450 × 9.70	2250	23	225	0.5d	22.2
	C-6	450 × 450 × 6.35	2250	35	337.5	0.75d	12.7
	C-7	300 × 300 × 6.35	1500	23	300	1.0d	12.7
Chicoine *et al*. (2002)	C-8	600 × 600 × 12.90	3000	23	600	1.0d	16
	C-9	600 × 600 × 12.90	3000	23	600	1.0d	16
	C-10	600 × 600 × 12.80	3000	23	300	0.5d	16
	C-11	600 × 600 × 9.70	3000	31	600	1.0d	16
Prickett and Driver (2006)	H1	400 × 400 × 7.98	2000	25	200	0.5d	12.8
	H2	400 × 400 × 8.00	2000	25	400	1.0d	15.9
	H3	400 × 400 × 7.99	2000	25	120	0.3d	12.8
	H4	400 × 400 × 8.01	2000	25	200	0.5d	12.8
	H5	400 × 400 × 8.02	2000	25	400	1.0d	15.9

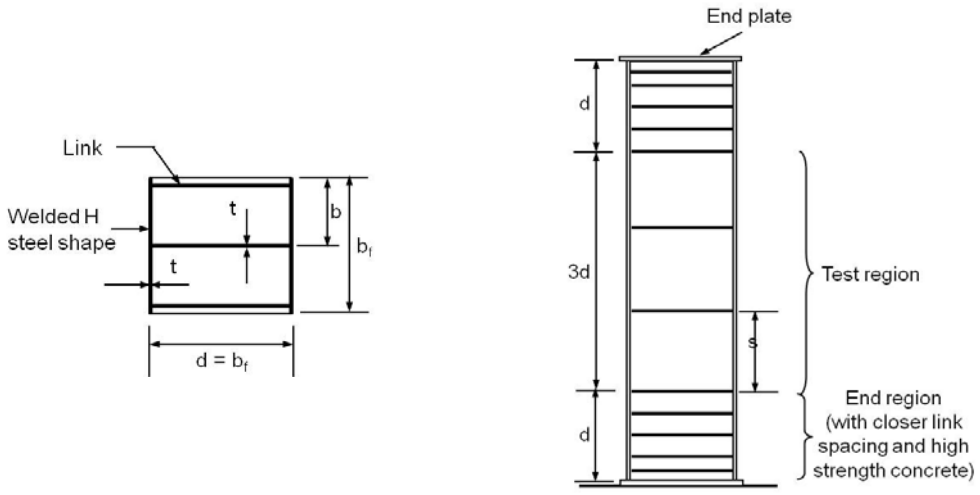

Fig. 3 Typical PEC test column: (a) cross-section; (b) elevation

where d is the depth of the cross-section. The flange plate slenderness (b/t) ratio varied between 23 and 35. Round mild steel bars of 12.7 mm diameter were used as transverse links in these columns, except specimen C-5 had larger bars of 22.2 mm diameter. Three different link spacings — 0.5d, 0.75d and 1.0d — were used in these columns. Specimens C-8 to C-11, tested by Chicoine *et al*. (2000), also under axial compression, were larger in their cross–sectional dimensions (600 mm × 600 mm) as compared to the previous test specimens. As shown in Table 1, most of the geometric properties for these specimens were similar, except specimen C-10, which had a link spacing of 0.5d and specimen C-11, which had a b/t ratio of 31.

Specimens H1 to H5, described in Table 1, are from the series of tests performed by Prickett and Driver (2006). These columns were 2000 mm long and had a cross-section of 400 mm × 400 mm with a flange width to thickness (b/t) ratio of 25. Three different link spacing values — 0.3d, 0.5d and 1.0d — were provided in these columns. The link diameter used was 12.7 mm and 16 mm, both satisfying the requirements of CSA S16-09 Clause 18.3.1 (CSA 2009). Among these five columns H1 and H2 were constructed using normal strength concrete whereas columns H3 to H5 is made of high strength concrete.

Table 2 provides the mechanical properties for the steel section and the test region concrete in these specimens. As shown in Fig. 3(b), the test region, where failure is forced to take place, is the central three–fifths region of the short PEC test specimens. High strength concrete and closer link spacing were used at the end regions of the columns to avoid local failure in those regions. The steel section was fabricated with CSA-G40.21-350W (CSA 2004) grade steel plate. Normal strength concrete PEC columns were cast with concrete having strength ranging from 28 to 34 MPa. High strength concrete of 60 MPa (nominal strength) was used in the end regions of these specimens to restrict failure to the test zones. However, the high strength concrete PEC columns have 60 MPa concrete in test region with a very high-strength concrete (nominally 80 MPa) in the end regions. The test region and end regions of the test specimen is shown in Fig. 3.

Table 2 Material properties of reference test specimens

Reference	Specimen	Properties of concrete				Properties of steel plate					
		f_{cu} (MPa)	E_c (MPa)	ε_{cu} ($\mu\varepsilon$)	v	F_y (MPa)	F_{sh} (MPa)	F_u (MPa)	ε_y (%)	ε_{sh} (%)	ε_u (%)
Tremblay *et al.* (1998)	C-2	32.7	28000	2250	0.18	370	370	519	0.19	1.87	15.20
	C-3	32.4	27800	2250	0.18	370	370	519	0.19	1.87	15.20
	C-4	31.9	28000	2250	0.18	370	370	519	0.19	1.87	15.20
	C-5	34.3	28800	2250	0.18	370	370	519	0.19	1.87	15.20
	C-6	33.1	28200	2250	0.18	374	374	519	0.19	1.87	15.20
	C-7	31.9	31500	2250	0.18	374	374	519	0.19	1.87	15.20
Chicoine *et al.* (2002)	C-8	34.2	27300	2000	0.18	360	360	519	0.19	1.87	15.20
	C-9	34.2	27300	2000	0.18	360	360	519	0.19	1.87	15.20
	C-10	34.2	27300	2000	0.18	360	360	519	0.19	1.87	15.20
	C-11	34.2	27300	2000	0.18	345	345	529	0.18	1.95	30.10
Prickett and Driver (2006)	H1	28.7	23300	2220	0.13	394	394	528	0.19	1.67	15.80
	H2	29.7	23300	2230	0.13	394	394	528	0.19	1.67	15.80
	H3	60.0	28000	2880	0.16	394	394	528	0.19	1.67	15.80
	H4	58.9	28800	2995	0.16	394	394	528	0.19	1.67	15.80
	H5	61.7	28500	3165	0.16	394	394	528	0.19	1.67	15.80

5. Finite element modelling

5.1 Geometric properties

The composite section of the reference test columns are first converted into their equivalent steel section. The equivalent steel columns are then analysed under concrentric loading conditions using ABAQUS finite element code (HKS 2007). In order to capture the local buckling behavior, S4R shell elements were used to model the steel plates. Each node of the S4R shell element has six degrees of freedom—three translations and three rotations. This element uses one integration point on its mid-surface to form the element internal force vector. The default number of integration points through the thickness of this element is five, which is considered sufficient for modelling the nonlinear material behaviour of the current problem. All plate elements in ABAQUS/Standard are based on an updated Lagrangian formulation (HKS 2007). This formulation is useful for the current problem because the elements experience considerable shape changes resulting from large rotations due to local buckling of the flange plates. To account for the shape change, the nodal coordinates are updated at the beginning of each increment to reflect current positions in space and all the shape functions and derivatives are re-evaluated using the updated nodal coordinates.

5.2 Material properties

The steel material properties for the equivalent steel section were modelled with an elasto-

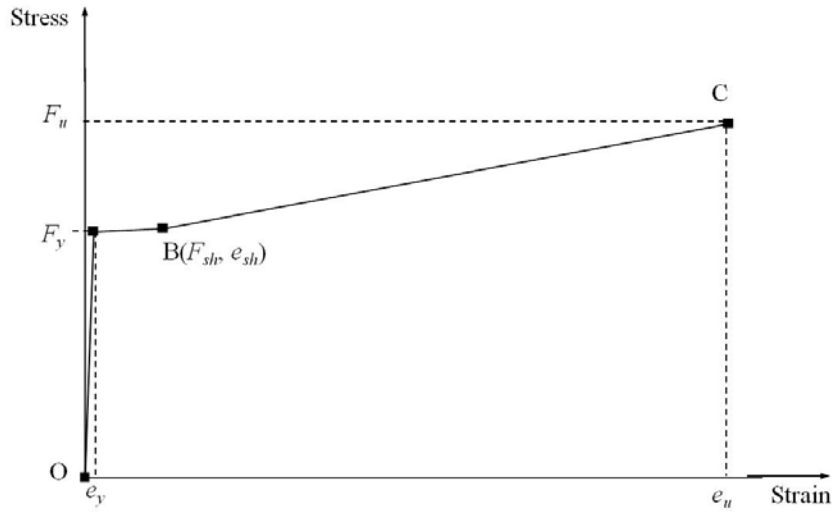

Fig. 4 Stress–Strain Curve for steel used in the numerical analysis

plastic J2 model. The stress–strain relationship for steel is defined as a trilinear curve, as shown in Fig. 4. Point A in the stress–strain curve is the yield point, point B refers to the onset of strain hardening and point C is the ultimate stress point. The material data used to define this trilinear curve for the steel plate material in the finite element analysis are listed in Table 2. These values are obtained from tensile tests on steel coupons from the test specimens (Tremblay *et al*. 1998, Chicoine *et al*. 2000, and Prickett and Driver 2006).

Since the model formulation is based on the updated Lagrangian description, the true (Cauchy) stress and logarithmic strain are needed to describe the effective stress–effective plastic strain. The stress and strain data obtained from the uniaxial tension tests are converted to true stress, σ_{true}, and logarithmic plastic strain, ε_{ln}^{pl}, using the following relationships (Lubliner *et al*. 1989)

$$\sigma_{true} = \sigma_{nom}(1 + \varepsilon_{nom}) \tag{19}$$

$$\varepsilon_{\ln}^{pl} = \ln(1 + \varepsilon_{nom}) - \frac{\sigma_{true}}{E_s} \tag{20}$$

where, E_s is the modulus of elasticity of steel, σ_{nom} is the nominal, or engineering, stress and ε_{nom} is the nominal, or engineering, strain obtained from material tests. The value of Poisson's ratio for steel used in the numerical analysis is 0.3.

5.3 Boundary conditions and solution strategy

Fixed boundary conditions are applied in the finite element model at the bottom of the column which is similar as that observed in the test specimens. The axial load was applied using displacement control technique at the top surface of the column. In the finite element model geometric nonlinearities are included along with the nonlinear material behaviour. Geometric

nonlinearities can occur due to the large displacement resulting from the local buckling of the flange plates. Newton-Raphson solution strategy is implemented to trace the nonlinear behaviour of the equivalent steel column under concentric axial loading only.

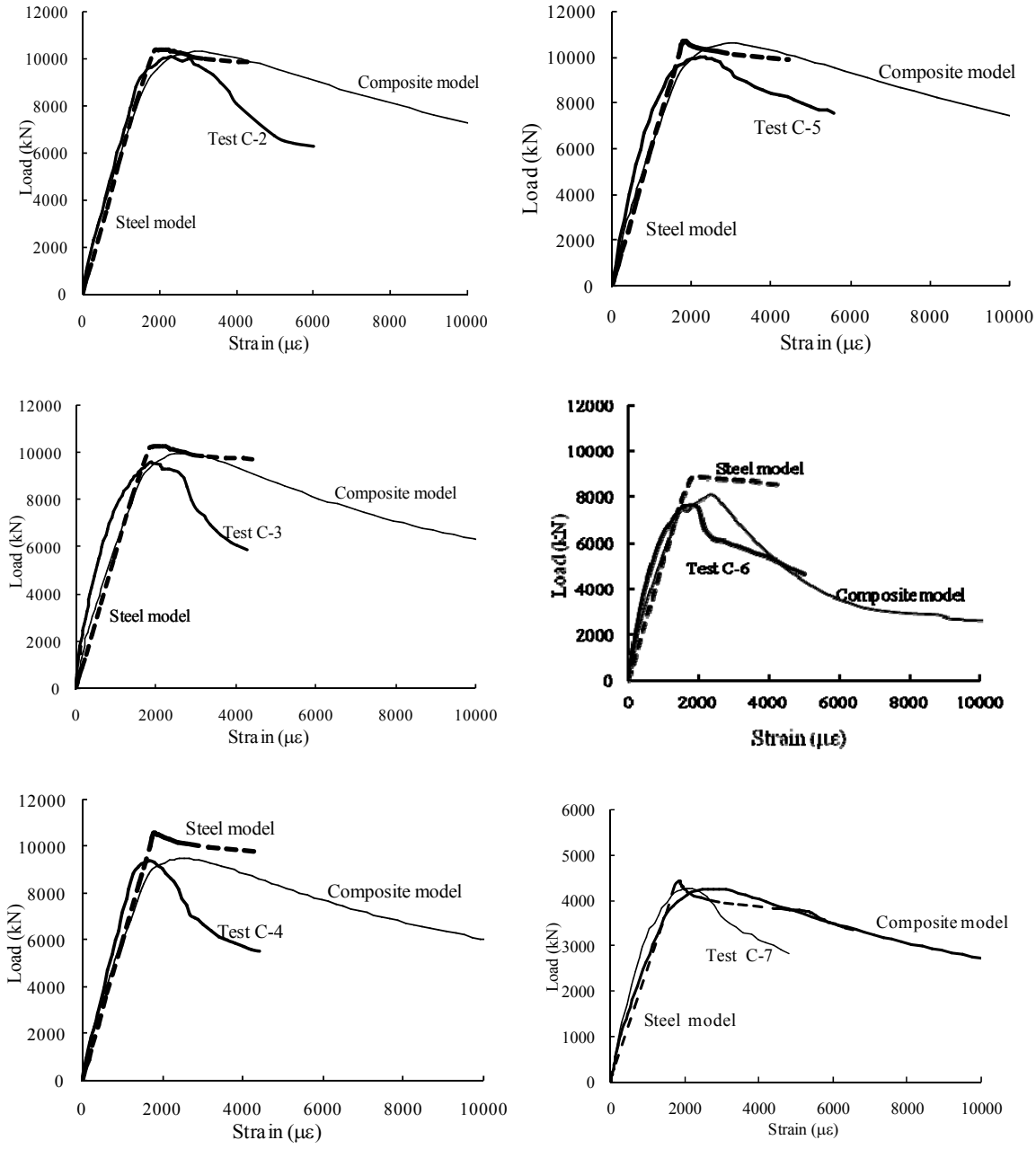

Fig. 5 Experimental and numerical load versus strain behaviour for PEC columns

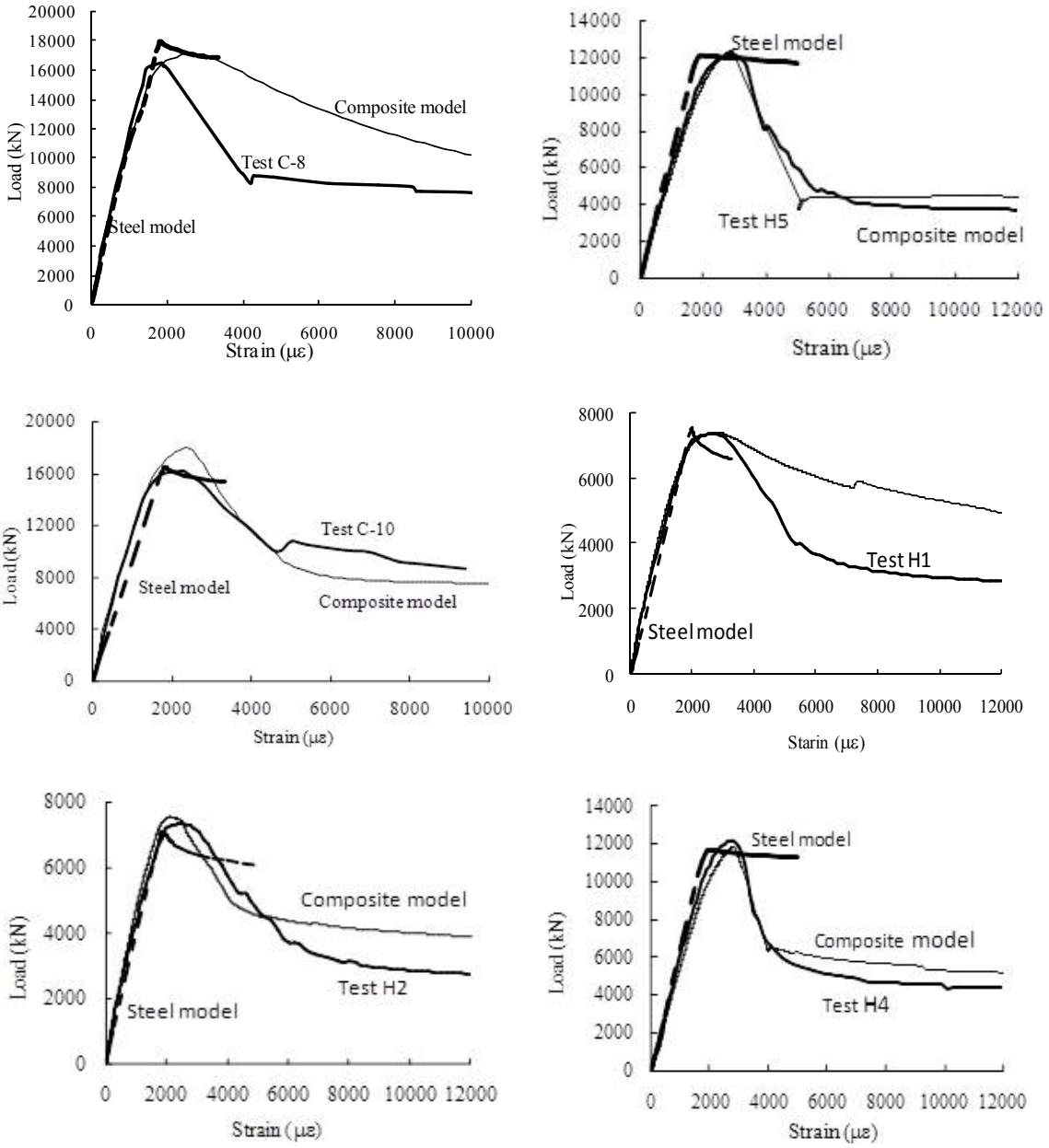

Fig. 5 Continued

6. Performance of the finite element model

The performance of the finite element model using equivalent steel section is evaluated comparing the results with that obtained from the experiments as well as with that obtained from

the finite element model (Begum *et al*. 2007) considering entire composite section of the column. Discussions on the results are included in the following sections.

6.1 Axial load versus strain behaviour

The numerical load versus average axial strain curves for the reference test columns are constructed from the numerical simulations of PEC columns using equivalent steel section and compared to that obtained from the composite FEM model (as developed by Begum *et al*. 2007) as well as to that obtained from the experiments. These curves for ten representative specimens are shown in Fig. 5. From the graphs it is clear that the initial portions of the numerical load vs. strain curves obtained from the steel model matched very well with the experimental ones as well as with that obtained from the composite model. The ultimate axial load point obtained from finite element model with equivalent steel section is found to be very close to the ultimate load of the test columns. However, some discrepancies are observed in the axial strain at the peak point. The axial strain obtained from the steel model corresponding to the peak load is found to be lower than the experimentally obtained peak strain value. Moreover, the descending branch of the load versus

Table 3 Performance of FEM model for PEC column with equivalent steel section

Specimen design.	Peak load			P_{exp}/P_{num}		Peak Strain			$\varepsilon_{exp}/\varepsilon_{num}$	
	Numerical		Exp.			Numerical		Exp.		
	Steel model P_{num} (kN)	Comp. model P_{num} (kN)	P_{exp} (kN)	Steel model	Comp. model	Steel model ε_{num} ($\mu\varepsilon$)	Comp. model ε_{num} ($\mu\varepsilon$)	ε_{exp} ($\mu\varepsilon$)	Steel model	Comp. model
C-2	10360	10230	10100	0.97	0.99	1880	2267	2306	1.23	1.02
C-3	10260	9920	9650	0.94	0.97	1960	1985	1920	0.98	0.97
C-4	10595	9190	9390	0.89	1.02	1810	1652	1695	0.94	1.03
C-5	10710	10350	10000	0.93	0.97	1900	2265	2330	1.23	1.03
C-6	8700	8100	7650	0.88	0.94	1880	1811	1763	0.94	0.97
C-7	4425	4110	4280	0.97	1.04	1890	2209	2142	1.13	0.97
C-8	17890	16540	16470	0.92	1.00	1805	1684	1845	1.02	1.10
C-9	17890	16540	16610	0.93	1.00	1805	1684	1770	0.98	1.05
C-10	16530	18030	16240	0.98	0.90	1800	2360	2256	1.25	0.96
C-11	14050	14280	14930	1.06	1.05	1760	1870	1810	1.03	0.97
H1	7095	7290	7383	1.04	1.01	1960	2510	2770	1.41	1.10
H2	7090	7355	7573	1.07	1.03	1910	2013	2081	1.09	1.03
H3	11760	12450	12340	1.05	0.99	2837	2890	3420	1.21	1.18
H4	11650	12150	11860	1.02	0.98	2190	2810	2835	1.29	1.01
H5	12050	12160	12390	1.03	1.02	2200	2890	2905	1.32	1.01
Mean*				0.98	0.99				1.13	1.03
SD*				0.06	0.04				0.14	0.06

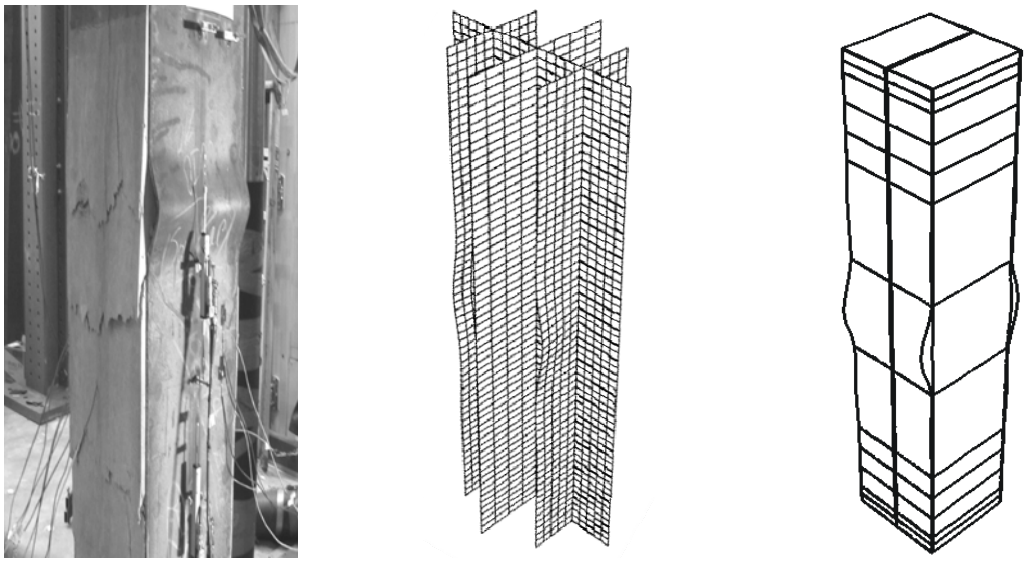

Fig. 6 Failure behaviour obtained from (a) Experiment (Prickett and Driver 2006); (b) FEM model with equivalent steel column; and (c) FEM model with composite column (Begum *et al*. 2007)

displacement curve obtained from FEM model with equivalent steel section deviates from the experimental load versus displacement curve. These discrepancies in the numerical strain values near and after the peak point can be attributed to the fact that in formulating the equivalent steel section the linear elastic material behaviour is assumed for steel plates. Material nonlinearity was not considered at all in the formulation, for keeping the model simple. The composite model provided more representative strain values as compared to the steel model at the cost of computational time and complexity.

6.2 Ultimate axial capacity

The comparisons between the ultimate axial capacities and corresponding average axial strains obtained from the numerical models and from the experiments are presented in Table 3. The ratio of the peak load of the test column to the equivalent steel column varied from 0.88 to 1.07 with an average value of 0.98 and a standard deviation of 0.06. The average axial strain values corresponding to the peak point, of the steel model is found to be much lower (as shown in Table 3) than the experimental peak strain values as well as the peak strains obtained from the composite model. The average value of the experimental to numerical strain ratio is 1.13 with a standard deviation of 0.14. These values were found to be 1.03 and 0.06, respectively when the experimentally obtained peak axial strain is compared to that obtained from the composite finite element model. The composite finite element model was developed with the entire composite section of the column using a sophisticated nonlinear material model for concrete and contact algorithm at the steel concrete interface. The accuracy of the composite FEM model for PEC column demonstrated by Begum *et al*. (2007) was found to be highly satisfactory. However, the model requires extensive theoretical knowledge and computational time. For design engineers this

imposes restrictions for using the complex model for their day to day design work. Though the steel model renders deviations in the strain values after the limit point it can easily be included in the commercially available design softwares and can save computational as well intellectual time of the design engineers.

6.3 Failure behaviour

The failure behaviour obtained from the finite element analysis using equivalent steel section is compared to that obtained from the experiments (Fig. 6(a)) and from the composite model. The ultimate capacity of the equivalent steel column was observed to attain by the occurrence of local buckling of the steel plates, as shown in Fig. 6(b), accompanied by yielding of steel at the same location. Similar behaviour was also observed in the steel plates of the test column (Fig. 6(a)) as well as in composite FEM model (Fig. 6(c)) at failure.

7. Conclusions

The composite cross–section of partially encased composite column is replaced by a fictitious section made entirely of steel. The fictitious steel section is restricted to consist of the entire steel section, with two additional steel plates representing the contribution of concrete and transverse links. The equivalent steel section was used to simulate the behaviour of partially encased composite columns under concentric gravity loading only. The effect of local buckling of the thin flanges was accounted through the implementation of effective width of the flange plates. The axial capacity obtained from the finite element simulation is compared to that obtained from the experiments on the reference test columns. The finite element simulations of the composite columns with equivalent steel sections are found to predict the experimental behaviour of PEC columns with very good accuracy up to the limit point. However, after the limit point the steel model renders lower strain values as compared to the experimentally obtained values due to the exclusion of material nonlinearities while formulating the fictitious steel section. Though the steel model renders deviations in the strain values after the limit point it can easily be included in the commercially available design softwares and can save computational as well intellectual time of the design engineers.

Acknowledgments

All assistance including laboratory, computing and financial supports from Bangladesh University of Engineering and Technology (BUET), Dhaka, Bangladesh are gratefully acknowledged.

References

Begum, M., Driver, R.G. and Elwi, A.E. (2007), "Finite element modeling of partially encased composite columns using the dynamic explicit solution method", *J. Struct. Eng.*, *ASCE*, **133**(3), 326-334.

Bouchereau, R. and Toupin, J.-D. (2003), "Étude du Comportement en Compression-Flexion des Poteaux Mixtes Partiellement Enrobés", *Report EPM/GCS-2003-03*, Department of Civil, Geological and Mining

Engineering, Ecole Polytechnique, Montreal, QC, Canada.
Chen, Y., Wang, T., Yang, J. and Zhao, X. (2010), "Test and numerical simulation of partially encased composite columns subject to axial and cyclic horizontal loads", *Int. J. Steel Struct.*, **10**(4), 385-393.
Chicoine, T., Massicotte, B. and Tremblay, R. (2003), "Long–term behavior and strength of partially-encased composite columns with built up shapes", *J. Struct. Eng., ASCE*, **129**(2), 141-150.
Chicoine, T., Tremblay, R. and Massicotte, B. (2002), "Finite element modelling and design of partially encased composite columns", *Steel Compos. Struct., Int. J.*, **2**(3), 171-194.
Chicoine, T., Tremblay, R., Massicotte, B., Yalcin, M., Ricles, J. and Lu, L.-W. (2000), "Test programme on partially-encased built up three-plate composite columns", *Joint Report EPM/GCS No. 00-06*, February, Department of Civil, Geological and Mining Engineering, Ecole Polytechnique, Montreal, Canada – ATLSS Engineering Research Centre, No. 00-04, Lehigh University, Bethlehem, PN, USA.
CSA (2004), "CSA G40.21-04, Structural Quality Steel", Canadian Standards Association, Rexdale, ON, Canada.
CSA (2009), "CSA S16-09, Limit States Design of Steel Structures", Canadian Standards Association, Toronto, ON, Canada.
Dastfan, M. (2011), "Ductile steel plate shear walls with PEC columns", Ph.D. Thesis, Department of Civil and Environmental Engineering, University of Alberta, Alberta, AB, Canada.
Deng, X., Dastfan, M. and Driver, R.G. (2008), "Behaviour of steel plate shear walls with composite columns", *Proceedings of American Society of Civil Engineers Structures Congress*, Vancouver, BC, Canada.
HKS (2003), Hibbitt, Karlsson and Sorensen, Inc., *ABAQUS / Standard User's Manual*, Version 6.3.
HKS (2007), Hibbitt, Karlsson and Sorensen, Inc., *ABAQUS / Analysis User's Manual*, Version 6.7.
Lubliner, J., Oliver, J., Oller, S. and Onate, E. (1989), "A plastic-damage model for concrete", *Int. J. Solids Struct.*, **25**(3), 229-326.
Maranda, R. (1998), "Analyses par Éléments Finis de Poteaux Mixtes Avec Sections d'acier En I de Classe 4", *Report n°. EPM/GCS-1998-11*, Department of Civil, Geological and Mining Engineering, Ecole Polytechnique, Montreal, QC, Canada.
Marinopoulou, A.A., Balopoulos, V.D. and Kalfas, C.N. (2007), "Simulation of partially encased composite steel-concrete columns with steel columns", *J. Construct. Steel Res.*, **63**(8), 1058-1065.
Prickett, B.S. and Driver, R.G. (2006), "Behaviour of partially encased composite columns made with high performance concrete", *Structural Engineering Report No. 262*, Department of Civil and Environmental Engineering, University of Alberta, AB, Canada.
Tremblay, R., Massicotte, B., Filion, I. and Maranda, R. (1998), "Experimental study on the behaviour of partially encased composite columns made with light welded h steel shapes under compressive axial loads", *Proceedings of SSRC Annual Technical Session & Meeting*, Atlanta, GA, USA, September, pp. 195-204.

CC

Notation

The following symbols are used in this paper:

A_{se}	=	effective area of the steel shape including the I section and the links
A_c	=	area of concrete section
A_a	=	area of the additional steel plates in fictitious section
b	=	half flange width
b_e	=	total effective width of the flange
b_f	=	full width of a flange plate
b_a, d_a, t_a	=	dimensions of additional steel plates
b_r, d_r	=	distance from centroidal axes
d	=	overall depth of the cross section
E_c	=	elastic modulus of concrete
E_s	=	Elastic modulus of steel
E_{se}	=	Elastic modulus of steel and links
$E_{c,eff}$	=	Effective elastic modulus of concrete
f_s	=	design stress of steel
f_c	=	design stress of concrete
f_{cu}	=	compressive strength of concrete
F_y	=	yield strength of steel plate
f_{sh}	=	stress at the onset of strain hardening of steel
F_u	=	ultimate strength of steel plate
l_a	=	moment of inertia of additional plates
$l_{c,y}$	=	moment of inertia of concrete in composite steel-concrete cross section about major axis
$l_{se,y}$	=	moment of inertia of the steel shape including the I section and the links about major axis
$l_{se,z}$	=	moment of inertia of the steel shape including the I section and the links about minor axis
m_{cd}	=	design- stress ratio for concrete-to-steel
m_{rd}	=	design-stress ration for reinforcement-to-steel
m_d	=	Normalized design stress of reinforced concrete
m_e	=	concrete to steel ratio of elasticity moduli
P_{exp}	=	experimental peak load
P_{num}	=	numerical peak load
s	=	transverse link spacing
t	=	plate thickness
n	=	1.5 as proposed by Chicoine *et al*. (2002)
ε_{cu}	=	compressive strain of concrete at ultimate point
ε_{sh}	=	strain at the onset of strain hardening of steel
ε_u	=	strain at the ultimate strength of steel
ε_y	=	yield strain of steel

ε_{exp} = experimental peak axial strain
ε_{num} = numerical peak axial strain
ϕ = transverse link diameter
λ_p = Slenderness parameter
λ_{se} = Normalized radii of gyration of steel cross-section
ρ_{se}, ρ'_{se} = Normalized area, $\rho_{se} = A_{se} / b_f d$, and its complement, $\rho'_{se} = 1 - \rho_{se}$
$\beta, \eta, \chi, \gamma$ = normalized plate dimensions, $\beta = b_a / b_f$; $\eta = t_a / d$; $\chi = d_a / d$ *and* $\gamma = t / b_f$